Monthly Notices of the ROYAL ASTRONOMICAL SOCIETY

MNRAS **541,** 4049–4059 (2025) https://doi.org/10.1093/mnras/staf1240
Advance Access publication 2025 July 28

Near-infrared characterization of evolved massive stars in M31 and M33

Michaela Kraus [1]★ María Laura Arias,[2,3] Michalis Kourniotis,[1] Andrea F. Torres,[2,3] Lydia S. Cidale[2,3] and Marcelo Borges Fernandes[4]

[1]*Astronomical Institute, Czech Academy of Sciences, Fričova 298, CZ-251 65 Ondřejov, Czech Republic*
[2]*Departamento de Espectroscopía, Facultad de Ciencias Astronómicas y Geofísicas, Universidad Nacional de La Plata, Paseo del Bosque S/N, La Plata B1900FWA, Buenos Aires, Argentina*
[3]*Instituto de Astrofísica de La Plata (CCT La Plata – CONICET, UNLP), Paseo del Bosque S/N, La Plata B1900FWA, Buenos Aires, Argentina*
[4]*Observatório Nacional, Rua General José Cristino 77, 20921-400 São Cristovão, Rio de Janeiro, Brazil*

Accepted 2025 July 25. Received 2025 July 24; in original form 2024 August 15

ABSTRACT

The upper region of the Hertzsprung–Russell diagram is populated by massive stars in a diversity of evolutionary stages, and the classification of these stars is often based on observed characteristics exclusively in the optical spectral range. The near-infrared regime provides useful complementary information that can help resolving ambiguities in stellar classification and add valuable information about circumstellar envelopes or late-type companions. We present new, near-infrared medium-resolution K-band spectra for a sample of six evolved massive stars, four in M31 and two in M33. The spectra are obtained with the Gemini Near-Infrared Spectrograph (GNIRS) at the Gemini North telescope. We detect CO band emission from the environment of two M31 objects, J004320.97+414039.6 and J004621.08+421308.2, which we classify as B[e] supergiants, with J004320.97+414039.6 being most likely in a post-red supergiant stage. Two objects have pure emission from the hydrogen Pfund series. Of these, we propose that J004415.00+420156.2 in M31 could also be a B[e] supergiant while J013410.93+303437.6 (Var 83) is a well-known luminous blue variable (LBV) in M33. The M31 star J004229.87+410551.8 has a featureless spectrum and its evolutionary stage remains inconclusive; it could be an LBV undergoing an S Dor cycle. The object J013242.26+302114.1 in M33 displays a pure absorption spectrum, including CO bands, consistent with its identification as a cool star. Radial velocity measurements of this red component, combined with modelling of the spectral energy distribution, suggest that J013242.26+302114.1 may be a binary system consisting of an LBV or B[e] supergiant primary and a red supergiant secondary. If confirmed, it would represent the first of its kind.

Key words: methods: observational – techniques: spectroscopic – circumstellar matter – stars: emission-line, Be – supergiants – stars: winds, outflows.

1 INTRODUCTION

Massive stars (>8 $M_\odot$) are the cornerstone to the dynamical and chemical evolution of their host galaxies. With their intense winds throughout the entire evolution and outburst activities in advanced evolutionary stages, massive stars enrich their environments with large quantities of chemically processed material and inject vast amounts of energy into them (e.g. Eldridge & Stanway 2022).

The upper part of the Hertzsprung–Russell (HR) diagram is populated with a plethora of objects displaying a variety of observational characteristics. In the blue region, we find classical blue supergiants (BSGs) along with B[e] supergiants (B[e]SGs) and Luminous Blue Variables (LBVs) in their quiescent state. Towards lower temperatures reside A- to G-type supergiants (YSGs) together with warm and yellow hypergiants (YHGs) as well as LBVs undergoing an S Dor cycle (also often referred to as 'LBV outburst'). The cool end of the HR diagram of massive stars is the home of the red supergiants (RSGs), but also YHGs that are in outburst can dwell in this temperature domain. To add to the zoo of evolved massive stars, the terminology of 'iron stars' or Fe II stars has been used in the literature to describe luminous hot stars that display a large amount of emission lines, predominantly Fe II and [Fe II], but often lack atmospheric absorption lines that would allow to classify the nature of the underlying star (Walborn & Fitzpatrick 2000; Clark et al. 2012; Humphreys et al. 2014). Such iron emission dominated spectra might represent LBVs in outburst but are also common for B[e]SGs.

To tell all these objects apart is not always an easy task, as their characteristics can change considerably during outburst phases, mimicking (some of) the properties of other object classes, and a lot of effort has been undertaken to define robust classification criteria for each object class (see e.g. Humphreys & Davidson 1994; Weis & Bomans 2020 for LBVs, Lamers et al. 1998; Kraus 2019 for B[e]SGs, de Jager 1998; Oudmaijer et al. 2009 for YHGs, and Humphreys et al. 2013 for warm hypergiants).

However, the evolutionary paths of massive stars from the main sequence to their deaths are yet most uncertain. Stellar evolution calculations critically depend on a variety of input parameters concerning the internal structure and physical processes, such as

★ E-mail: michaela.kraus@asu.cas.cz

mixing and core-overshooting, metallicity, initial rotation, and the star's mass-loss behaviour along the entire evolution (Heger & Langer 2000; Heger, Langer & Woosley 2000; Ekström et al. 2012; Georgy, Saio & Meynet 2014; Groh et al. 2014; Szécsi et al. 2022). Many of these parameters cannot be (easily) accessed from observations, and inaccurate determinations of input parameter values can lead to huge uncertainties in the predictions from evolutionary models (Martins & Palacios 2013). Furthermore, possible or likely evolutionary connections between, for example, YHGs, warm hypergiants, B[e]SGs and LBVs are not yet fully established. It is also still unclear to what extent binary interaction affects the observed phenomena and, despite some progress made (Kraus 2019; Mahy et al. 2022; Marchant & Bodensteiner 2024; Kourniotis et al. 2025), there is still insufficient information on the multiplicity within the individual classes. Nevertheless, observations of the diverse objects help characterizing their class and evolutionary state. Discoveries of new members lead to more profound insight on massive star populations in these extreme evolutionary transition phases and on the evolutionary and dynamically history of massive stars in different host galaxies.

The luminous stellar population of a galaxy sticks out due to the high optical brightness of its members, which makes it easier to identify them, and which makes studies of extragalactic objects highly attractive. In the past decades, many surveys were dedicated to resolve the diverse massive star populations in galaxies within and beyond the Local Group by means of optical spectroscopy (Humphreys, Massey & Freedman 1990; Corral 1996; Fabrika & Sholukhova 1999; Fabrika et al. 2005; Valeev, Sholukhova & Fabrika 2009; Clark et al. 2012; Humphreys et al. 2013, 2014, 2017a, b; Gordon, Humphreys & Jones 2016; Kourniotis et al. 2017; Solovyeva et al. 2019; Dorn-Wallenstein, Neugent & Levesque 2023; Sholukhova et al. 2024), including tools based on machine learning (Maravelias et al. 2022), or by optical spectroscopy combined with multiband photometry (Massey et al. 1996, 2007, 2014; Massey, Neugent & Smart 2016; Humphreys et al. 2019; Maravelias et al. 2023; Bonanos et al. 2024). The identified objects were classified based on common characteristics and similarities with representatives of their classes in the Milky Way.

However, the classification of massive stars based solely on optical spectroscopy and multiband photometry bears ambiguities, because stars in different evolutionary states can display very similar spectra with only subtle differences. In addition, an infrared excess detected in the spectral energy distribution can be caused by either circumstellar dust or a late-type companion (or a combination of both). Therefore, complementary information is needed to unambiguously classify a star and its environment.

A number of surveys of evolved massive stars have been carried out in the near-infrared spectral range revealing a great diversity of spectroscopic features, including emission from warm molecular gas from circumstellar environments (McGregor, Hyland & Hillier 1988a; McGregor, Hillier & Hyland 1988b; McGregor, Hyland & McGinn 1989; Hanson, Conti & Rieke 1996; Morris et al. 1996). Follow-up investigations by Oksala et al. (2013) were dedicated to specifically unveil the near-infrared properties of YHGs, LBVs, and B[e]SGs, and to characterize their envelopes and (where appropriate) circumstellar discs. This study provided complementary information to discriminate between LBV candidates (cLBV) and B[e]SGs, as these share many characteristics at optical wavelengths. Combining the characteristics of these two classes of evolved massive stars from the optical and infrared spectral regions with information about their infrared colours resulted in a more reliable classification of objects (Kraus et al. 2014; Kraus 2019) and the identification of new candidates to both classes of objects (e.g. Sholukhova et al. 2015; Kourniotis et al. 2018; Cochetti et al. 2020).

Motivated by this, we started to systematically observe extragalactic luminous stars with ambiguous classification in the near-infrared spectral domain with the aim to improve the classification of the objects and to study their environments. To achieve this, we mainly focus on detecting emission from the CO first overtone bands. These molecular bands are an immediate indication for a dense and warm (< 5000 K) circumstellar environment (McGregor et al. 1988a; Kraus 2009). Detection of emission from the CO bands serves as a complementary criterion to classify a star as B[e]SG (Kraus et al. 2014) rather than as cLBV, although we note that only about 50 per cent of the B[e]SGs show these bands (Oksala et al. 2012, 2013; Kraus 2019). Conversely, the absence of CO band emission does not automatically exclude the B[e]SG nature of the object. If detected, the CO bands have a further advantage, because they consist of emission from the isotopes ^{12}CO and ^{13}CO, and their ratio indicates whether the star was already evolved or yet unevolved at the time of ejection of the material (Kraus 2009; Liermann et al. 2010).

In this work, we present medium-resolution *K*-band spectra of six objects listed in Table 1, one being a proposed LBV star in M33. Five of the objects have literature classification as either cLBV, iron star (Fe II), B[e]SG, or warm hypergiant, based on studies of their optical spectral characteristics, photometric variability, and spectral energy distribution. Four of these objects reside in M31 and one in M33. For four objects, these are the first near-infrared spectra.

2 OBSERVATIONS AND DATA REDUCTION

Medium-resolution ($R \sim 5900$) *K*-band spectra of our objects were obtained with the Gemini Near-InfraRed Spectrograph (GNIRS; Elias et al. 2006a, b) attached to the 8.1-m telescope at Gemini North Observatory. Data acquisition was between January 2019 and September 2020 with the short camera (0.15 arcsec pixel^{-1}), a slit width of 0.3 arcsec, and the 111 l/mm grating centred at 2.3 μm for a wavelength coverage of 2.2–2.4 μm. The observations were carried out in AB pairs to facilitate sky subtraction. Data reduction was performed using standard IRAF[1] tasks. The individual steps include flat-fielding, wavelength calibration, and removal of telluric features.

To perform the telluric correction, spatially close-by late B- or early A-type main-sequence stars were observed immediately before or after the target exposure at similar airmass. Choosing telluric standard stars in this narrow spectral-type range has the advantage that the telluric star itself has no intrinsic spectral features in the observed spectral region (2.2–2.4 μm). Their spectra hence serve as perfect template for correcting the science spectra from telluric absorption features. The selected telluric stars are also bright ($K = 6$–7 mag), allowing to obtain a spectrum with significant signal-to-noise (S/N) ratios (typically 100–200) with short exposures. The telluric correction was performed with the IRAF task *telluric*, which enables interactive scaling and wavelength shifting of the telluric standard spectrum to achieve optimal cancellation of the atmospheric (telluric) features in the target spectrum.

Finally, the spectra were normalized by fitting the continuum with low-order polynomial. S/N ratios of the spectra are 33 (J004229.87+410551.8), 90 (J004415.00+420156.2), 16 (J004320.97+414039.6), 52 (J004621.08+421308.2), 82 (J013242.26+302114.1), and 28 (J013410.93+303437.6).

[1]IRAF is distributed by the National Optical Astronomy Observatory, which is operated by the Association of Universities for Research in Astronomy (AURA) under cooperative agreement with the National Science Foundation.

Table 1. Objects and proposed classifications from literature and ours.

Galaxy	Object LGGS	Alternative SIMBAD identifier	V (mag)	K (mag)	Literature classification	Reference	New classification
M31	J004229.87+410551.8	–	18.785	13.90	cLBV / FeII / B[e]SG	1, 2, 3	LBV in S Dor cycle?
M31	J004415.00+420156.2	BA 1–621	18.291	14.54	cLBV / FeII / B[e]SG	1, 2, 3	B[e]SG
M31	J004320.97+414039.6	BA 1–558	19.215	15.20	cLBV / FeII / B[e]SG	4, 2, 3	post-RSG B[e]SG
M31	J004621.08+421308.2	[WB92a] 895	18.155	15.15	cLBV / warm hypergiant	4, 5	B[e]SG
M33	J013242.26+302114.1	IFM-B 57	17.440	13.88	cLBV / FeII / B[e]SG	1, 6, 3	cLBV/B[e]SG + RSG?
M33	J013410.93+303437.6	IFM-B 1588, VHK 83[a]	16.027	15.26	LBV	7	LBV

Notes. [a] formerly Var 83. V-band and K-band magnitudes are from Massey et al. (2006) and the 2MASS survey and catalogue (Cutri et al. 2003; Skrutskie et al. 2006), respectively, except for the K-band magnitude for J004229.87+410551.8, which is from Peacock et al. (2010). References: (1) Massey et al. (2007), (2) Humphreys et al. (2014), (3) Humphreys et al. (2017a), (4) King, Walterbos & Braun (1998), (5) Gordon et al. (2016), (6) Clark et al. (2012), (7) van den Bergh, Herbst & Kowal (1975).

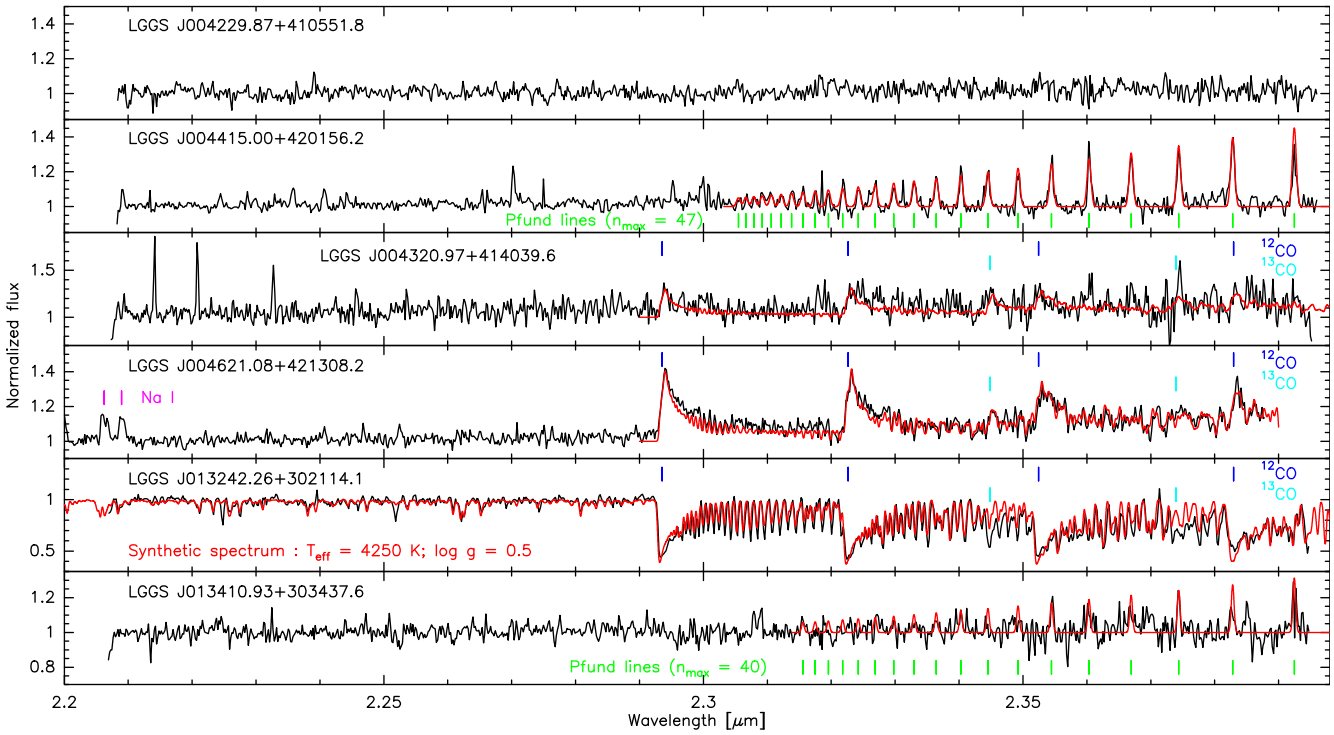

Figure 1. Best-fitting model to the circumstellar emission and absorption seen in the normalized GNIRS spectra of our objects. The parameters for the CO band and Pfund line emission are listed in Tables 2 and 3, respectively. The parameters for the atmospheric model are listed in the corresponding panel. The order of the objects follows the one in Table 1.

Details on our targets are listed in Table 1, where we provide the name of the host galaxy, the identifier of the object from the Local Group Galaxies Survey (LGGS; Massey et al. 2006) along with their archival V- and K-band photometry and previous classifications found in the literature.

3 RESULTS

The normalized spectra, shifted to the rest wavelength,[2] are shown in Fig. 1. We detect CO band emission from J004320.97+414039.6 and J004621.08+421308.2, CO band absorption in J013242.26+302114.1, emission from the hydrogen Pfund series from J004415.00+420156.2 and J013410.93+303437.6, while the spectrum of J004229.87+410551.8 appears to be featureless.[3] In the following, we model the emission from the CO bands and from the Pfund series to derive the physical parameters (temperature, density, dynamics) of the circumstellar environment of these objects.

3.1 CO band emission

The positions of the individual band heads of both ^{12}CO and ^{13}CO are indicated with vertical bars in Fig. 1. The observed shape of the CO band heads with a blue-shifted shoulder and a red-shifted

[2]Except for J004229.87+410551.8 because the spectrum contains no reference line to determine the shift.

[3]The same telluric standard star spectrum has been used to clean the spectra of J004229.87+410551.8 and J004415.00+420156.2 (as it was observed in between the two target exposures) and in both science spectra the telluric features were equally good and completely removed. We also checked that the K-band spectrum is not contaminated by the near-by cluster (Kang et al. 2012) as the cluster is well separated from the object on the acquisition image and does not fall into the slit. Hence, the featureless spectrum of J004229.87+410551.8 is real.

Table 2. Best-fitting parameters of the CO band emission.

Object LGGS	T_{CO} (K)	N_{CO} (cm^{-2})	$^{12}CO/^{13}CO$	$v_{rot,los}$ ($km\,s^{-1}$)	v_{Gauss} ($km\,s^{-1}$)
J004320.97+414039.6	2200±100	$(3\pm1)\times10^{21}$	3±1	60±10	2±0.5
J004621.08+421308.2	1500±100	$(5\pm1)\times10^{22}$	50±10	60±10	2±0.5

maximum is characteristic of (Keplerian) rotation (Carr 1995; Kraus 2019) in a disc (or ring) revolving around the star. But it might also indicate equatorial outflow at constant velocity, which generates the same double-peaked profiles for the individual ro-vibrational lines as rotation (e.g. Kraus, Borges Fernandes & de Araújo 2010). In either case, the shape of the band heads suggests that the CO gas around J004320.97+414039.6 and J004621.08+421308.2 is most likely concentrated in a ring around the object, similar to what is typically found for B[e]SGs (Cidale et al. 2012; Muratore et al. 2012, 2015; Kraus et al. 2013, 2023). Furthermore, the analysis of multiple disc tracers demonstrated that B[e]SGs are surrounded by multiple rings of gas and dust in (quasi-) Keplerian rotation (Aret et al. 2012; Kraus et al. 2016; Maravelias et al. 2018; Torres et al. 2018). Therefore, we assume that the CO gas around our targets is also rotating.

To generate synthetic CO band spectra, we utilize our code developed by Kraus et al. (2000) to compute the emission of ^{12}CO from a Keplerian rotating disc, and advanced by Kraus (2009) and Oksala et al. (2013) by adding ^{13}CO. In addition, we have implemented updated values for the energy levels and Einstein transition coefficients for both ^{12}CO and ^{13}CO from Li et al. (2015). The code computes the CO band emission under the assumption of local thermodynamic equilibrium conditions. This is a reasonable assumption given the high column densities usually found in these molecular rings. The best-fitting parameters are listed in Table 2, and the fits are included in Fig. 1. The parameters T_{CO} and N_{CO} denote the temperature and column density of the CO gas, and the gas dynamics is represented by the rotation velocity projected to the line of sight, $v_{rot,los}$, and a Gaussian component, v_{Gauss}, combining the contributions from the thermal and turbulent motions. The value for the abundance ratio of the molecular isotopes $^{12}CO/^{13}CO$ marks the amount of enrichment of the circumstellar environment in ^{13}C. This value mirrors the stellar surface isotope abundance ratio $^{12}C/^{13}C$ at the time of material ejection from the star. The atomic isotopic abundance ratio has an initial (interstellar) value of about 90 and gradually decreases during stellar evolution. This is shown in Fig. 2 for evolutionary tracks of a star at solar metallicity (which is similar to the metallicity of M31) with an initial mass of $20\,M_\odot$ and for rotation rates $\Omega/\Omega_{crit} = 0.1 - 0.5$ in steps of 0.1 (Ekström et al. 2012). The tracks are interpolations obtained by the tool SYCLIST[4] (Yusof et al. 2022). With increasing rotation velocity of the star, the enrichment in ^{13}C on the stellar surface starts earlier in the evolution, but values of the abundance ratio below 5 occur only after the star has passed through the RSG phase. The shown tracks approximately represent the evolution of our two objects with CO band emission, for which luminosities of $\log L/L_\odot = 5.0 - 5.1$ have been determined (Humphreys et al. 2014; Gordon et al. 2016). The derived CO abundance ratios indicate that the environments of both stars are enriched in ^{13}CO.

We emphasize that the parameters for J004320.97+414039.6 bear some uncertainty due to the very weak CO signal compared to the noise and significant remnants of telluric lines polluting the red portion of the spectrum. Nevertheless, the high enrichment in ^{13}CO in the spectrum of this object appears to be real, and the low errorbar in the abundance ratio of the CO isotopes (despite the lower quality of the spectrum) is due to the significantly increased sensitivity of the emission spectrum with increasing ^{13}CO abundance.

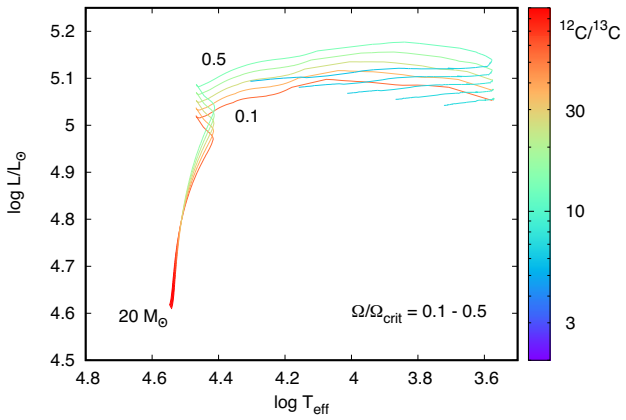

Figure 2. Stellar evolution tracks for rotating stars with solar metallicity and initial mass of $20\,M_\odot$. Tracks are interpolations of those computed by Ekström et al. (2012). The change in abundance ratio of the carbon isotopes during the evolution is indicated. For all rotation rates, values below 5 are clearly reached only after the stars have passed through the RSG evolution.

In contrast, J004621.08+421308.2 is found to have a low ^{13}CO abundance and the value of $^{12}CO/^{13}CO$ is less well constrained, resulting in a considerably larger errorbar. On the other hand, the star's environment has a significantly higher CO column density than J004320.97+414039.6. This higher column density results in an increase in optical depth across the ^{12}CO band heads and, consequently, in a reduced relative flux ratio between the ^{12}CO and ^{13}CO band heads. Therefore, the ^{13}CO band heads become prominent in the observed spectrum despite the 50 times lower column density of the ^{13}CO gas.

3.2 Pfund line emission

In contrast to the CO bands, the Pfund lines detected in J004415.00+420156.2 and J013410.93+303437.6 display single-peaked profiles suggesting that the lines form in the ionized wind rather than in a rotating or outflowing disc. The maximum detectable Pfund line, n_{max}, is an indicator for the hydrogen density, N_H, in the line-forming region. We use the code developed by Kraus et al. (2000) which adopts Menzel's case B recombination, fix the electron temperature at 10 000 K, which is a typical value in the winds of B-type supergiants,[5] and assume that the lines are optically thin

[4] https://www.unige.ch/sciences/astro/evolution/en/database/syclist/

[5] A slightly higher or lower electron temperature does not affect the resulting shape of the emission spectrum, just the total line intensities. But these differences disappear when normalizing the synthetic spectra.

Table 3. Best-fitting parameters for the emission of the Pfund series.

Object LGGS	N_H (cm^{-3})	n_{max}	v_{Gauss} ($km\,s^{-1}$)
J004415.00+420156.2	$(1.9\pm0.3)\times10^{13}$	47	60±10
J013410.93+303437.6	$(4.9\pm0.7)\times10^{13}$	40	60±10

and their profile shapes can be represented with a Gaussian profile. The best-fitting parameters for the hydrogen density, maximum number of detected Pfund line, and kinematics are listed in Table 3, and the fits are included in Fig. 1. The parameters derived for J013410.93+303437.6 should be treated with caution because the spectrum exhibits a high noise level compared to the intensity of the emission lines and some remnants of telluric lines are present in the red part of the spectrum. Due to the high noise level, the maximum detectable Pfund line might be higher (lower). Consequently, the hydrogen density within the line forming region might be a lower (upper) limit.

3.3 Absorption spectra

The object J013242.26+302114.1 presents a pure absorption spectrum with very intense CO bands in the portion of the *K*-band region covered by our observations. CO bands in absorption are typically seen from the photospheres of late-type stars, which could mean that a cool object appears on the same sky position as the hot supergiant star J013242.26+302114.1.[6] To verify this, we computed models with the spectrum synthesis code Turbospectrum using MARCS atmospheric models (Plez 2012). Unfortunately, these atmosphere models contain only ^{12}CO whereas the observed spectrum shows clear indication for intense ^{13}CO as well. Therefore, we include in Fig. 1 a synthetic spectrum for pure demonstration purpose, not with the aim to have the best-fitting model. We find that the general spectral features are decently well represented with an effective temperature between 4000 and 4250 K and a log *g* in the range 0.5–1.0. However, these temperature values should be regarded as upper limit, because any contribution to the near-infrared continuum emission from either a hot component or circumstellar dust reduces the observable line intensities, meaning that the real temperature of the cool component will be lower.

4 DISCUSSION

The *K*-band spectra of the six studied objects display a large diversity. Nevertheless, when combining the new information with what is known about the objects from the literature, they help address the question of classification, at least for those stars with distinct emission features.

4.1 Objects in M31

4.1.1 An LBV in an S Dor cycle?

The object J004229.87+410551.8 has been classified by Massey et al. (2007) as a hot cLBV. According to their definition, a hot cLBV is a star with an optical spectrum resembling the one of an LBV in its visual minimum and thus its quiescent S Dor phase. This means that the optical spectrum displays intense emission of the Balmer lines and of singly ionized metals, primarily [Fe II]. In contrast, Humphreys et al. (2014) used the numerous iron emission lines as a criterion to classify the object as a Fe II star, whereas later-on Humphreys et al. (2017b) proposed a B[e]SG status due to the infrared excess seen with data from *Spitzer* and WISE. However, the star is in a crowded region (Massey et al. 2016), and as mentioned by Humphreys et al. (2014), a cluster is at only 1 arcsec separation to J004229.87+410551.8. Because both *Spitzer* IRAC and WISE have low angular resolution (2 arcsec and more than 6 arcsec, respectively), a contamination of the stellar infrared fluxes cannot be excluded. Based on this, a B[e]SG status of J004229.87+410551.8 has already been questioned by Kraus (2019). Our featureless *K*-band spectrum adds further evidence that the star is not a classical B[e]SG, because B[e]SGs typically display either intense Pfund line emission, or CO band emission, or both. Galactic as well as Magellanic Cloud B[e]SGs with CO band emission populate the luminosity range $\log L/L_\odot \sim 5.0 - 5.9$ (Oksala et al. 2013; Kraus 2019; Kraus et al. 2023). With a luminosity of J004229.87+410551.8 of $\log L/L_\odot \simeq 5.2$ (Humphreys et al. 2014), the star falls well into this range. The absence of both Pfund line and CO band emission suggests that neither the wind nor the equatorial environment of the star are dense enough to create detectable emission. Therefore, we tentatively exclude a B[e]SG classification of the object.

We also consider the hypothesis that J004229.87+410551.8 might be an LBV candidate, as proposed by Massey et al. (2007). The *K*-band survey of Oksala et al. (2013) revealed that LBVs display intense Pfund line emission when they are in their hot, quiescent state, while they show a featureless (e.g. LHA 120-S 155) or an absorption spectrum mimicking a cool (A- to F-type) supergiant star (e.g. WRAY 15–751) when they are in outburst. The absence of Pfund line emission seems to speak against an LBV in quiescence. To check whether J004229.87+410551.8 could be in outburst, the star should show a brightening. The data base of the Zwicky Transient Facility (ZTF) photometric survey (Bellm et al. 2019; Masci et al. 2019) provides observations of J004229.87+410551.8 through data release DR23.[7] These observations were conducted in the optical *g* band between June 2018 and October 2024. Furthermore, we inspected the catalogue of *BVRI* photometric observations of luminous stars in M31 collected between August 2012 and November 2023 at the UIS Henry Barber Research Observatory,[8] of which the results from the first four years of monitoring have been published by Martin & Humphreys (2017). Fig. 3 shows the time series of the observations with the date of our observations marked. The photometric measurements in all bands display a scatter of about 0.2–0.3 mag around the average magnitude, which might indicate some low-amplitude quasi-periodic variability. We also added the photometric measurements of Massey et al. (2006) from September 2002 and marked the dates of spectroscopic observations taken in September 2002 (Massey et al. 2007) and in October 2010 (Humphreys et al. 2014). These data clearly demonstrate that in 2002 the star was dimmer (∼0.8 mag in *B*, ∼1 mag in *V*, ∼2 mag in *I*) and bluer ($B-V=0.27$ in 2002 versus 0.62 in 2023; $V-I=0.35$ in 2002 versus 1.18 in 2023). Brightening and simultaneous reddening are typical characteristics of an S Dor variability (Weis & Bomans 2020). This suggests that J004229.87+410551.8 might have entered an S Dor cycle somewhen between the last optical spectroscopic observation in 2010 and the beginning of the photometric monitoring in 2012 and that it is stable since then. The duration of S Dor cycles can spread from years to

[6]Our acquisition image showed only a single point-source object at the position of J013242.26+302114.1.

[7]https://irsa.ipac.caltech.edu/Missions/ztf.html

[8]https://uisacad5.uis.edu/jmart5/M31M33photcat/

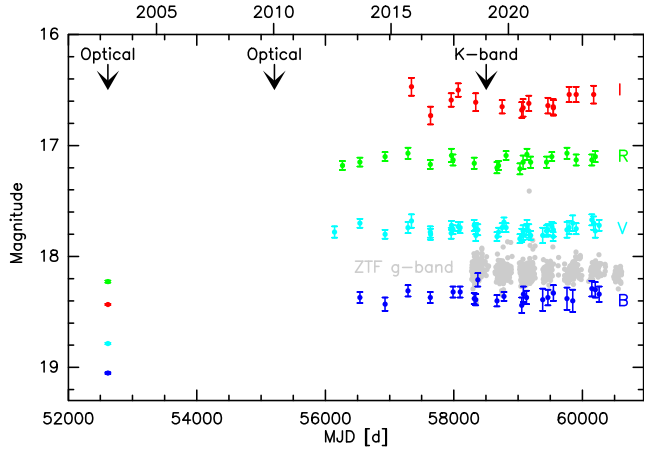

Figure 3. Time series observations of J004229.87+410551.8 collected in g band with ZTF and $BVRI$ filters. For clarity of the plot, the error bars of the ZTF measurements (which are of similar size as for the $BVRI$ photometry) are omitted. The errorbars of the data from 2002 are smaller than the symbol size. The arrows mark the dates of spectroscopic observations in the optical (Massey et al. 2007; Humphreys et al. 2014) and in the K band (ours).

decades (Weis & Bomans 2020). To confirm or refute this and to further follow the evolution of this object, new optical spectroscopic observations combined with new multiband photometry are urgently needed.

4.1.2 B[e] supergiants

The objects J004415.00+420156.2 and J004320.97+414039.6 have previously also been classified as (hot) cLBVs by Massey et al. (2007) and King et al. (1998), as Fe II stars by Humphreys et al. (2014), and as B[e]SGs by Humphreys et al. (2017b). Likewise, a B[e]SG status was proposed for both objects by Kraus (2019) due to their infrared colours, which clearly separate them from the region populated by LBVs in the colour–colour diagrams. Optical and near-infrared spectra of J004415.00+420156.2 have also been presented by Sarkisyan et al. (2020) who found clear indication of free–free and free–bound emission from an ionized wind. From the presented data it is inconclusive whether emission from the Pfund series is seen in their spectrum, and the authors do not mention it. Our K-band spectrum of J004415.00+420156.2 displays only emission from the Pfund series. However, its high luminosity of $\log(L/L_\odot) = 5.73$ (Humphreys et al. 2014) aligns the star with high-luminosity B[e]SGs (LHA 120-S 22, LHA 120-S 127) in the Large Magellanic Cloud (LMC) lacking CO band emission (Kraus 2019). In contrast, J004320.97+414039.6 displays weak CO band emission. With its luminosity of $\log(L/L_\odot) = 5.01$ (Humphreys et al. 2014), it resides at the lower luminosity border of B[e]SGs showing CO band emission (Kraus 2019). The strong enrichment in ^{13}CO suggests an evolved, presumably post-red supergiant evolutionary state, but a better quality spectrum would be required to confirm this.

The last object in our M31 sample is J004621.08+421308.2. It was suggested to be a cLBV by King et al. (1998), whereas Gordon et al. (2016) proposed it could belong to the group of warm hypergiants with an infrared excess. While Gordon et al. (2016) state that the stellar spectrum would indicate a late A spectral type due to the absence of He I emission, they assign the star an effective temperature of ~ 9000 K and a spectral type A0 in their table 4. Follow-up optical and near-infrared spectroscopic observations were carried out by Sarkisyan et al. (2020), who reported the detection of CO band emission from that star. Their spectrum has somewhat lower resolution than our GNIRS spectrum and covers only the first two band heads of ^{12}CO, which makes it difficult to estimate the physical parameters of the CO emitting region. Nevertheless, the molecular emission seems to be persistent, as we also detected it in our spectrum taken about 8 yr later. While the CO temperature obtained from our modelling is lower than what is found in most discs around B[e]SGs, it is comparable to the Galactic B[e]SG star MWC 349 (Kraus et al. 2020). Intense and persistent CO band emission is characteristic for many B[e]SGs, while it is only occasionally seen in YHGs (see Kraus et al. 2023, for an overview). The revised stellar temperature 10 000 − 15 000 K by Sarkisyan et al. (2020) from both their spectrum (that shows He I emission) and spectral energy distribution (SED) modelling, agrees with a spectral-type B so that we tentatively classify the star as a B[e]SG. The rather low enrichment in ^{13}CO seen in our spectrum speaks in favour of a star that is only slightly evolved (pre-RSG) at the time of material ejection. The small wavelength shift of our spectrum of J004621.08+421308.2 allows us to detect also intense emission from the Na I doublet. These emission lines are reported from the environments of many evolved massive stars, such as YHGs (Lambert, Hinkle & Hall 1981; Oudmaijer & de Wit 2013; Clark, Negueruela & González-Fernández 2014; Kourniotis et al. 2017; Koumpia et al. 2022; Kraus et al. 2023), most B[e]SGs (McGregor et al. 1988b; Oksala et al. 2013; Arias et al. 2021), but also LBVs in their cool (i.e. active or outburst) phase (Oksala et al. 2013). Therefore, their presence does not impose any further constraints on the evolutionary state of an object. However, we point out that the reported change in the behaviour of the He I lines in the optical spectrum is certainly worth being further monitored.

4.2 Objects in M33

4.2.1 The LBV star Var 83

Turning to the objects in M33, we start with J013410.93+303437.6, which is also known as M33 Var 83 detected by den Bergh et al. (1975) as a Hubble & Sandage (1953) variable. With a luminosity of $\log(L/L_\odot) = 6.3$ (Humphreys et al. 2014), J013410.93+303437.6 is clearly more luminous than all known B[e]SGs. Its optical emission-line spectrum has been described by Humphreys (1978) who found close similarity of its spectral appearance with other luminous and variable stars in M31 and M33. From then on, this star was listed as an LBV. To our knowledge, it never underwent an LBV-typical eruption that would justify this clear classification, but it displays infrared emission, in particular at 8 μm, that offsets the star from the region occupied by classical LBVs in the infrared colour–colour diagram (Clark et al. 2012) and might suggest warm dust in its environment.

Some clues to the likely LBV nature of the star are provided by the multi-epoch $BVRI$ photometry, shown in Fig. 4. The measurements are taken from the catalogue for luminous stars in M33[9] and spread over about 12 yr (from July 2012 to February 2024). The light curves display irregular brightness variations of 0.7–0.8 mag in all bands with no or only mild colour variations. And a V-band variability with an amplitude of 0.71 mag was already reported by Martin & Humphreys (2017). The brightening event that started beyond MJD = 57000 d is similar in amplitude to the one detected in the years 1981–1982 (Szeifert et al. 1996). But in this recent event, it lasted for about 5 yr. Such brightness variations, with durations of years

[9] https://uisacad5.uis.edu/jmart5/M31M33photcat/

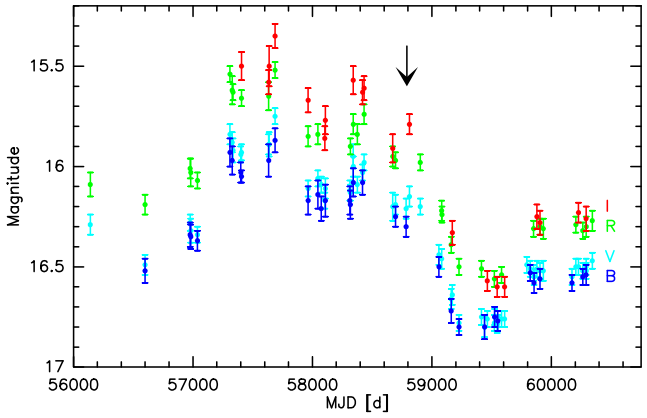

Figure 4. Time series observations of J013410.93+303437.6 (Var 83) collected in *BVRI* filters. The arrow marks the date of our *K*-band observations.

to decades, are typically observed in LBVs and known as S Dor cycles (Weis & Bomans 2020). As mentioned before, these S Dor cycles are usually accompanied by a spectroscopic change from an earlier to a later spectral type. However, spectroscopic observations of J013410.93+303437.6 are sparse. Interestingly, Humphreys et al. (2017a) reported stronger P Cygni profiles in the He I lines in the years 2013 and 2014, i.e. during quiescence before the brightening, compared to their spectrum taken in 2010. Unfortunately, the light curve does not date back to 2010, so that we cannot be sure whether the star was also in a brighter stage in 2010. Previous *V*-band measurements cover the years 2000−2003 when the magnitude showed only a mild scatter of ±0.1 mag around the average value of 16.44 mag (Shporer & Mazeh 2006).

The time of our observations was after the maximum brightness when the star was approaching again its quiescent state, which explains the *K*-band appearance with Pfund-line emission typical for a hot, luminous object. The emission from the hydrogen Pfund series that we detect is rather weak but comparable to the one of the similarly luminous LBV star LHA 120-S 128 in the LMC (Oksala et al. 2013). Consequently, our observations align well with the likely classification of J013410.93+303437.6 as an LBV.

4.2.2 *A red supergiant binary with a massive companion?*

The last of our targets is J013242.26+302114.1. Its spectrum displays clear and pure indication of a late-type star. No emission is detected, which complicates a refined classification of the star. The object has been previously classified based on its optical appearance, mainly in the blue spectral region, as a (hot) cLBV by Massey et al. (2007), as an iron star by Clark et al. (2012), and as a B[e]SG by Humphreys et al. (2017a).

Clark et al. (2012) report clear spectral variability over a 4-yr period for J013242.26+302114.1, in particular a change in emission line ratios of the Balmer lines. Their blue optical spectrum, acquired in September 2010, clearly indicates that the star is a hot, emission-line supergiant. These authors also noted photometric variability with an amplitude of $\Delta V \sim 0.8$ mag with no periodicity detected so far (see also Massey et al. 2007), and that the star's mid-infrared colours suggest a wind plus photosphere rather than circumstellar dust. As Kraus (2019) points out, the near-infrared colours place the star in the region of late-type stars, and she removed J013242.26+302114.1 from the list of B[e]SGs. Interestingly, Drout, Massey & Meynet (2012) classify J013242.26+302114.1 as RSG based on the star's location in colour–colour diagrams and the strengths of the Ca II

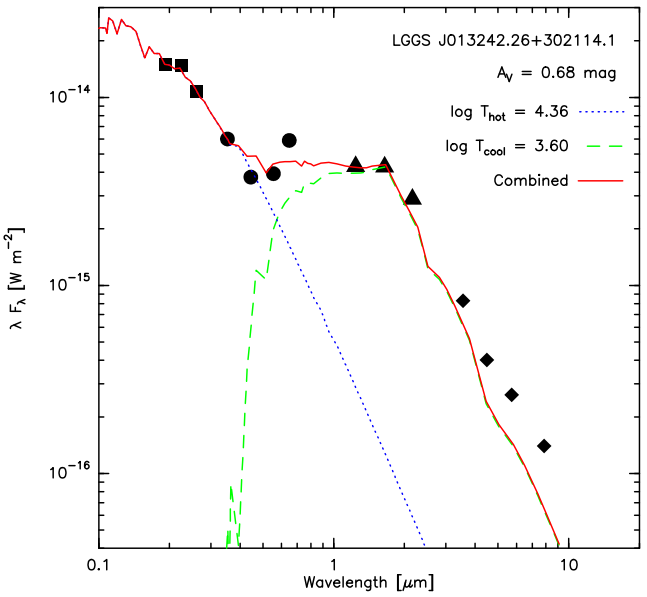

Figure 5. Dereddened SED of J013242.26+302114.1, consisting of a hot object and a RSG. Photometric data are from the UV catalogue (Yershov 2014, squares), the UBVR survey (Massey et al. 2006, circles), the 2MASS catalogue (Cutri et al. 2003, triangles), and the *Spitzer Space Telescope* (Khan et al. 2015, diamonds).

triplet lines and the O Iλ7774 line seen in their red spectra taken in 2010 November 26/27. Our *K*-band spectrum from January 2019 confirms the presence of a RSG. Therefore, we propose J013242.26+302114.1 could be a binary system consisting of a hot emission-line object and a RSG companion.

To test this hypothesis, we inspect the SED of J013242.26+302114.1 to see whether a RSG could be present in the data. For this purpose, photometric data were collected from various sources. We utilize the UV catalogue of Yershov (2014), optical photometry from Massey et al. (2006), near-infrared data from the Two Micron All Sky Survey (2MASS) catalogue (Cutri et al. 2003; Skrutskie et al. 2006) and mid-infrared measurements from the *Spitzer Space Telescope* (Khan et al. 2015). We excluded the measurements from WISE, because the star is in a crowded region (Massey et al. 2016). For dereddening, we apply the extinction curve of Cardelli, Clayton & Mathis (1989) with a value of $R_V = 3.2$. To represent the stellar continuum, we use models from the grid of continuum spectra computed by Kurucz (1992). We find a good match of the UV and blue optical range for an effective temperature of $T_{\rm eff,hot} = 22\,000 - 24\,000$ K and an extinction value of $A_V = 0.65 - 0.7$ mag. These parameters are similar to the ones obtained by Humphreys et al. (2017b).

The dereddened SED of J013242.26+302114.1 is plotted in Fig. 5. It clearly shows excess emission in the near- and mid-infrared, pointing towards the presence of a RSG. The model, which was fit to the blue part of the SED, is shown as dotted line. On the cool end, the Kurucz grid is sparse. To represent the RSG star with parameters close to what we estimate from the *K*-band spectrum, we utilize the model for $T_{\rm eff} = 4000$ K (which is the minimum temperature of the Kurucz grid) and $\log g = 1.0$. This model is added as the dashed line, and the curve for the combined models is shown with the solid line. Obviously, the inclusion of the RSG allows to fit the long-wavelength part of the SED fairly well. Moreover, the SED implies that the *K*-band region as well as the red optical region (longwards of 0.7 μm) is dominated by the RSG whereas the hot star dominates the

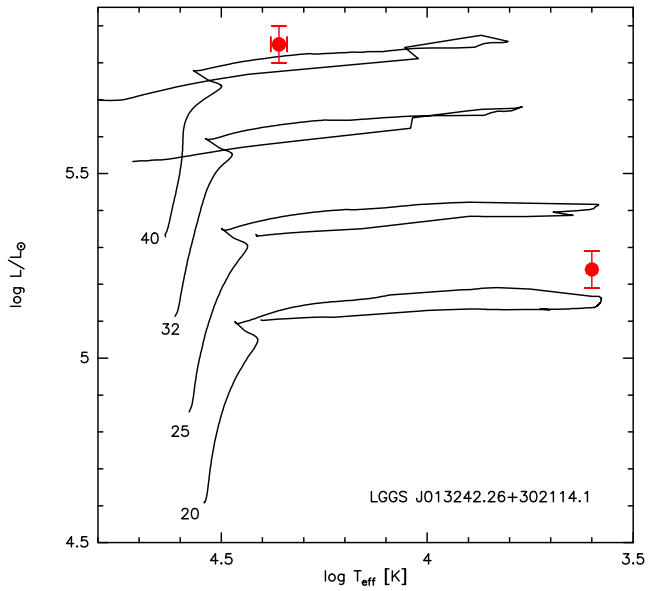

Figure 6. Location of the hot and cool components of J013242.26+302114.1 in the HR diagram along with evolutionary tracks for rotating stars with solar metallicity (from Ekström et al. 2012).

blue spectral region. This explains why Drout et al. (2012) identified J013242.26+302114.1 as a RSG based on their spectra, whereas Humphreys et al. (2014) could see only the signature of the hot star in their blue spectrum.[10]

From the SED fitting, and assuming a distance to M33 of 968 ± 50 kpc (U et al. 2009), we estimate stellar luminosities of $\log L_{\rm hot}/{\rm L}_\odot = 5.85 \pm 0.05$ and $\log L_{\rm cool}/{\rm L}_\odot = 5.24 \pm 0.05$ for the hot and cool components, respectively. Fig. 6 shows the positions of the two stars in the HR diagram along with stellar evolutionary tracks. A binary scenario might be possible if the massive component is an evolved, post-RSG star. In that case, the evolutionary tracks of rotating stars in the initial mass range of 40–45 $M_\odot$ postulate an age of about 5.4–5.8 Myr and a current mass of $M_{\rm hot} \simeq 20 - 22\,{\rm M}_\odot$ while the RSG age and mass would be on the order of 8.9–9.3 Myr and $M_{\rm cool} = 16.0 - 16.5\,{\rm M}_\odot$, respectively, when considering evolutionary tracks for rotating stars in an initial mass range of 21–22 $M_\odot$. While not the same, the ages for these single-star evolution scenarios have at least the same order of magnitude. The deviation from exact coeval evolution of the two components is similar to that found, for example, for a number of RSG binary components in the Small Magellanic Cloud (Patrick et al. 2024).

To affirm the binarity of J013242.26+302114.1, information about radial velocities is required. Unfortunately, no radial velocity measurements of the hot component exist, since the blue spectral region displays solely emission lines whose radial velocities do not necessarily reflect the dynamics of the hidden object.[11] However, in the frame of the second survey of the Apache Point Observatory Galactic Evolution Experiment (APOGEE-2), the RSG star has been observed multiple times between 2017 October 30 and 2019 November 13. High-resolution ($R \sim 22\,500$) spectra were collected in the near-infrared H-band (1.51–1.70 μm) range and radial velocity measurements were provided by this survey (Abdurro'uf et al. 2022). Furthermore, Drout et al. (2012) had measured the radial velocity of the RSG in their red optical spectrum, and we measured it in our K-band spectrum. All values are listed in Table 4 and shown in Fig. 7 as a function of time. The RSG presents clear radial velocity variations that might support the binary hypothesis.

Table 4. Radial velocity measurements for the RSG component in J013242.26+302114.1.

MJD (d)	$v_{\rm rad}$ (km s^{-1})	$\Delta v_{\rm rad}$ (km s^{-1})	Source
55527.	−121.6	–	Drout et al. (2012)
58056.70240	−110.8	<0.2	APOGEE-2
58059.69937	−110.8	<0.2	APOGEE-2
58059.87737	−110.7	<0.2	APOGEE-2
58060.80436	−110.7	<0.2	APOGEE-2
58067.84922	−110.9	<0.2	APOGEE-2
58084.74756	−110.4	<0.2	APOGEE-2
58085.62552	−110.3	<0.2	APOGEE-2
58086.57947	−110.3	<0.2	APOGEE-2
58450.81452	−103.6	<0.2	APOGEE-2
58504.72323	−100.0	4.0	GNIRS
58767.71925	−107.3	<0.2	APOGEE-2
58769.77429	−107.1	<0.2	APOGEE-2
58770.73831	−106.5	<0.2	APOGEE-2

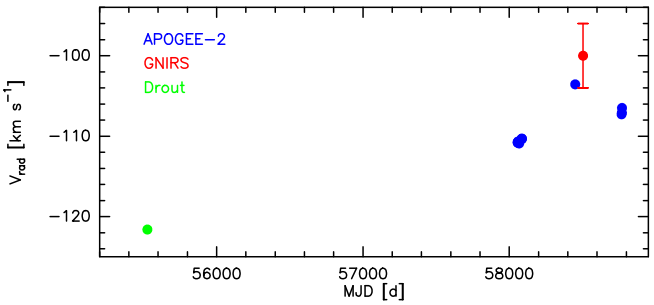

Figure 7. Radial velocity curve of the RSG component in J013242.26+302114.1.

The measurements are too sparse to reliably model the radial velocity curve, but based on the values from APOGEE-2 and Drout et al. (2012) we may claim that the semi-amplitude of the velocity of the RSG is at least $\sim 9\,{\rm km\,s^{-1}}$. Moreover, we can estimate the minimum orbital period $P_{\rm orb,min}$, by requesting that the semi-major axis (orbital separation), a, of the binary system should be larger than the sum of the radii of the two stars. With radii of the hot and cool components of $R_{\rm hot} \simeq 53\,{\rm R}_\odot$ and $R_{\rm cool} \simeq 867\,{\rm R}_\odot$, respectively, the minimum orbital separation is $a_{\rm min} = R_{\rm hot} + R_{\rm cool} \simeq 4.28$ au and we obtain $P_{\rm orb,min} = 2\pi\sqrt{a_{\rm min}^3/(GM_{\rm tot})} \simeq 532$ d, if we use for the total mass an average value of $M_{\rm tot} \simeq 37\,{\rm M}_\odot$. From the stellar radii and assumed current masses of the two components, we can infer that the orbital separation of the binary must be larger

[10] Although the red spectrum available at http://etacar.umn.edu/LuminousStars/M31M33/M31stars.html, which was not discussed by Humphreys et al. (2014), appears to exhibit the molecular absorption bands of TiO typical for RSGs in the spectral range 7050 –7300 Å.

[11] A low-resolution (69 km s^{-1} per pixel) optical spectrum covering the wavelength range 3700–9100 Å was observed with LAMOST (Luo et al. 2022). It displays clearly the composite features of a hot emission-line star and a RSG. However, we observed a systematic wavelength shift between emission lines in the blue and the green region on the order of 15 km s^{-1} that might indicate wavelength calibration uncertainties. Therefore, we refrain from using this spectrum for radial velocity measurements.

than the sum of the two stellar radii to satisfy the condition $a = (M_{\rm total}/M_{\rm hot})\,a_{\rm cool} = 1.76\,a_{\rm cool}$, or equivalently, $a_{\rm cool} = 0.57\,a$, where $a_{\rm cool}$ is the distance of the RSG to the centre of mass. Furthermore, utilizing the equation proposed by Eggleton (1983) for determining the effective radius of the Roche lobe, $R_{\rm L}$, of the RSG, we find a value of $R_{\rm L,cool} = 0.82\,a$ which is significantly larger than $a_{\rm cool}$, meaning that the star is not filling its Roche lobe. This, in turn, agrees with the about coeval evolution of the two components in which binary interaction has not played a (significant) role in the history of this object.

If J013242.26+302114.1 is indeed a binary with a luminous hot primary and a RSG secondary component, this would be an extremely interesting object because it would be one of the rare cases of a system with an evolved primary. The RSG binaries identified so far in the Milky Way and galaxies of the Local Group consist of a RSG primary and a B-type main sequence secondary (e.g. Neugent, Levesque & Massey 2018; Neugent et al. 2019, 2020, 2021; Pantaleoni González et al. 2020; Patrick et al. 2022, 2024). Such systems are to be expected from an evolutionary perspective, since companions with a lower mass than a B-type main-sequence star have not yet had enough time to reach the main sequence, while more massive companions evolve so quickly that it is rather unlikely to catch them at the right moment (see for example the discussion in Neugent et al. 2020). Also, many massive binaries merge before their primary even reaches the RSG stage, which explains why the currently known RSG binary fractions range from about 20 per cent in the low-metallicity environment of the Small Magellanic Cloud (Patrick et al. 2022) to about 40 per cent in the high-metallicity inner region of M33 (Neugent 2021) compared to the fraction of massive binaries on the main sequence, that is at least twice as high (e.g. Sana et al. 2012). Only two RSG binary systems are known with a different (non-main sequence) companion. These are the high-mass X-ray binary system 4U 1954+31 consisting of a RSG and a neutron star (Hinkle et al. 2020) and V766 Cen consisting of a RSG and a cool giant or supergiant (Wittkowski et al. 2017). Hence, finding systems with different companion stars, in particular more massive ones, may help shedding light on the properties of massive binary components in such extreme evolutionary stages and their final fate.

While it is tempting to predict J013242.26+302114.1 as the first RSG binary with an LBV/B[e]SG primary, we wish to caution that the reported radial velocity variations might also have a different origin. It is well known that RSGs have semiperiodic or irregular light variability possibly due to the interplay of radial pulsations and motions of major convection cells, as was proposed for Betelgeuse (Gray 2008). Periods were found to range from hundreds to thousands of days (e.g. Kiss, Szabó & Bedding 2006; Chatys et al. 2019) and radial velocity variations of up to $\sim 10\,{\rm km\,s^{-1}}$ have been detected in numerous RSGs (e.g. Josselin & Plez 2007; Soraisam et al. 2018) and were predicted by 1D pulsation test models (Arroyo-Torres et al. 2015). The radial pulsations in RSGs follow a period–luminosity relation according to which J013242.26+302114.1, having a K-band absolute magnitude of $M_K \sim -11$ mag, is expected to experience radial pulsations with a period of 500–1000 d (Kiss et al. 2006; Chatys et al. 2019). Due to this ambiguity, follow-up observations of J013242.26+302114.1 are urgently needed to complete the radial velocity curve, confirm that the hot, massive star is indeed the companion and not just a line-of-sight projection, and if confirmed, constrain the orbital parameters and stellar masses that may shed light on the evolutionary history of this interesting object. For this, UV spectroscopy might help to characterize the hot component in J013242.26+302114.1 (Patrick et al. 2024) and to measure its radial velocity.

5 CONCLUSIONS

We have carried out a K-band spectroscopic survey of six evolved massive stars in M31 and M33. Five of them had previously uncertain or controversial classification and one is an LBV. We have detected dense and warm molecular gas rings around two objects in M31 (J004320.97+414039.6 and J004621.08+421308.2) that we classify as B[e]SGs. Modelling the CO band emission revealed the physical properties (temperature, column density, gas dynamics) of the line-forming regions in these rings together with information about the surface enrichment in ^{13}C of the star at the time when the material, forming these rings, was ejected. Based on the measured high enrichment for J004320.97+414039.6, we conclude that the star is most likely in post-RSG evolution. We have detected a dense ionized wind from the M31 star J004415.00+420156.2 that we also consider as B[e]SG and a weaker one from the LBV star J013410.93+303437.6 (Var 83) in M33. The latter object just returned from an S Dor cycle at the time of our observations, explaining possibly the weaker wind observed. For the M31 object J004229.87+410551.8 with the featureless near-infrared spectrum, we investigated whether it could be a B[e]SG or an LBV. The lack of K-band features together with a constant brightness make it difficult to unambiguously determine the true nature of the object. However, the inspection of its previous photometry suggests that the star may be an LBV undergoing an S Dor cycle. In addition, we discovered that J013242.26+302114.1 in M33 is most likely a binary system consisting of a hot B-type emission-line object, which could be a post-RSG in an LBV or a B[e]SG phase, and a RSG companion. If confirmed, it would be the first RSG binary with a massive LBV/B[e]SG primary. Follow-up measurements are therefore urgently needed to complete the so far sparsely populated radial velocity curve and to validate the binary over the pulsation scenario. Once the orbital parameters are constrained, they could provide insight into the evolutionary history and possible fate of this interesting object.

The presented data and analyses reinforce that near-infrared spectra add significant information that helps classifying evolved massive stars, characterizing circumstellar environments, as well as identifying late-type companions, which can be missed out from the optical observations.

ACKNOWLEDGEMENTS

We thank the reviewer, Lee Patrick, for valuable comments and suggestions on the manuscript.

This paper is based on observations obtained at the international Gemini Observatory, a programme of NSF NOIRLab, which is managed by the Association of Universities for Research in Astronomy (AURA) under a cooperative agreement with the U.S. National Science Foundation on behalf of the Gemini Observatory partnership: the U.S. National Science Foundation (United States), National Research Council (Canada), Agencia Nacional de Investigación y Desarrollo (Chile), Ministerio de Ciencia, Tecnología e Innovación (Argentina), Ministério da Ciência, Tecnologia e Inovações (Brazil), and Korea Astronomy and Space Science Institute (Republic of Korea) under programme IDs GN-2018B-Q-301, GN-2019B-Q-201, and GN-2020B-Q-230.

This research made use of the NASA Astrophysics Data System (ADS), of the SIMBAD data base, operated at CDS, Strasbourg, France, of data products from the Two Micron All Sky Survey, which is a joint project of the University of Massachusetts and the Infrared Processing and Analysis Center/California Institute of Technology, funded by the National Aeronautics and Space Administration and

the National Science Foundation, and of data from the Zwicky Transient Facility (ZTF). The ZTF is supported by the National Science Foundation under Grants No. AST-1440341 and AST-2034437 and a collaboration including current partners Caltech, IPAC, the Weizmann Institute of Science, the Oskar Klein Center at Stockholm University, the University of Maryland, Deutsches Elektronen-Synchrotron and Humboldt University, the TANGO Consortium of Taiwan, the University of Wisconsin at Milwaukee, Trinity College Dublin, Lawrence Livermore National Laboratories, IN2P3, University of Warwick, Ruhr University Bochum, Northwestern University and former partners the University of Washington, Los Alamos National Laboratories, and Lawrence Berkeley National Laboratories. Operations are conducted by COO, IPAC, and UW. This research has made use of the VizieR catalogue access tool, CDS, Strasbourg, France (DOI : 10.26093/cds/vizier). The original description of the VizieR service was published in 2000, A&AS 143, 23.

The Astronomical Institute of the Czech Academy of Sciences is supported by the project RVO:67985815. MLA and AFT acknowledge financial support from CONICET (PIP 1337) and the Universidad Nacional de La Plata (Programa de Incentivos 11/G192), Argentina. MBF acknowledges financial support from the National Council for Scientific and Technological Development–CNPq – Brazil (grant number: 307711/2022-6). This project has received funding from the European Union's Framework Programme for Research and Innovation Horizon 2020 (2014-2020) under the Marie Skłodowska-Curie Actions Grant Agreement No. 823734 (POEMS) and from the European Union (project No. 101183150 - OCEANS).

DATA AVAILABILITY

The observed GNIRS *K*-band spectra can be retrieved from the publicly available Gemini Observatory Archive (https://archive.gemini.edu). The processed spectra will be shared on a reasonable request to the corresponding author.

REFERENCES

Abdurro'uf et al., 2022, ApJS, 259, 35
Aret A., Kraus M., Muratore M. F., Borges Fernandes M., 2012, MNRAS, 423, 284
Arias M. L., Vallverdú R., Torres A. F., Kraus M., 2021, Boletin de la Asociacion Argentina de Astronomia La Plata Argentina, 62, 104
Arroyo-Torres B. et al., 2015, A&A, 575, A50
Bellm E. C. et al., 2019, PASP, 131, 068003
Bonanos A. Z. et al., 2024, A&A, 686, A77
Cardelli J. A., Clayton G. C., Mathis J. S., 1989, ApJ, 345, 245
Carr J. S., 1995, Ap&SS, 224, 25
Chatys F. W., Bedding T. R., Murphy S. J., Kiss L. L., Dobie D., Grindlay J. E., 2019, MNRAS, 487, 4832
Cidale L. S. et al., 2012, A&A, 548, A72
Clark J. S., Castro N., Garcia M., Herrero A., Najarro F., Negueruela I., Ritchie B. W., Smith K. T., 2012, A&A, 541, A146
Clark J. S., Negueruela I., González-Fernández C., 2014, A&A, 561, A15
Cochetti Y. R., Kraus M., Arias M. L., Cidale L. S., Eenmäe T., Liimets T., Torres A. F., Djupvik A. A., 2020, AJ, 160, 166
Corral L. J., 1996, AJ, 112, 1450
Cutri R. M. et al., 2003, VizieR Online Data Catalog: 2MASS All-Sky Catalog of Point Sources. II/246
de Jager C., 1998, A&AR, 8, 145
Dorn-Wallenstein T. Z., Neugent K. F., Levesque E. M., 2023, ApJ, 959, 102
Drout M. R., Massey P., Meynet G., 2012, ApJ, 750, 97
Eggleton P. P., 1983, ApJ, 268, 368
Ekström S. et al., 2012, A&A, 537, A146
Eldridge J. J., Stanway E. R., 2022, ARA&A, 60, 455
Elias J. H., Rodgers B., Joyce R. R., Lazo M., Doppmann G., Winge C., Rodríguez-Ardila A., 2006a, in McLean I. S., Iye M., eds, Proc. SPIE Conf. Ser. Vol. 6269, Ground-based and Airborne Instrumentation for Astronomy. SPIE, Bellingham, p. 626914
Elias J. H., Joyce R. R., Liang M., Muller G. P., Hileman E. A., George J. R., 2006b, in McLean I. S., Iye M., eds, Proc. SPIE Conf. Ser. Vol. 6269, Ground-based and Airborne Instrumentation for Astronomy. SPIE, Bellingham, p. 62694C
Fabrika S., Sholukhova O., 1999, A&AS, 140, 309
Fabrika S., Sholukhova O., Becker T., Afanasiev V., Roth M., Sanchez S. F., 2005, A&A, 437, 217
Georgy C., Saio H., Meynet G., 2014, MNRAS, 439, L6
Gordon M. S., Humphreys R. M., Jones T. J., 2016, ApJ, 825, 50
Gray D. F., 2008, AJ, 135, 1450
Groh J. H., Meynet G., Ekström S., Georgy C., 2014, A&A, 564, A30
Hanson M. M., Conti P. S., Rieke M. J., 1996, ApJS, 107, 281
Heger A., Langer N., 2000, ApJ, 544, 1016
Heger A., Langer N., Woosley S. E., 2000, ApJ, 528, 368
Hinkle K. H., Lebzelter T., Fekel F. C., Straniero O., Joyce R. R., Prato L., Karnath N., Habel N., 2020, ApJ, 904, 143
Hubble E., Sandage A., 1953, ApJ, 118, 353
Humphreys R. M., 1978, ApJ, 219, 445
Humphreys R. M., Davidson K., 1994, PASP, 106, 1025
Humphreys R. M., Massey P., Freedman W. L., 1990, AJ, 99, 84
Humphreys R. M., Davidson K., Grammer S., Kneeland N., Martin J. C., Weis K., Burggraf B., 2013, ApJ, 773, 46
Humphreys R. M., Weis K., Davidson K., Bomans D. J., Burggraf B., 2014, ApJ, 790, 48
Humphreys R. M., Gordon M. S., Martin J. C., Weis K., Hahn D., 2017a, ApJ, 836, 64
Humphreys R. M., Davidson K., Hahn D., Martin J. C., Weis K., 2017b, ApJ, 844, 40
Humphreys R. M., Stangl S., Gordon M. S., Davidson K., Grammer S. H., 2019, AJ, 157, 22
Josselin E., Plez B., 2007, A&A, 469, 671
Kang Y., Rey S.-C., Bianchi L., Lee K., Kim Y., Sohn S. T., 2012, ApJS, 199, 37
Khan R., Stanek K. Z., Kochanek C. S., Sonneborn G., 2015, ApJS, 219, 42
King N. L., Walterbos R. A. M., Braun R., 1998, ApJ, 507, 210
Kiss L. L., Szabó G. M., Bedding T. R., 2006, MNRAS, 372, 1721
Koumpia E., Oudmaijer R. D., de Wit W. J., Mérand A., Black J. H., Ababakr K. M., 2022, MNRAS, 515, 2766
Kourniotis M., Bonanos A. Z., Yuan W., Macri L. M., Garcia-Alvarez D., Lee C. H., 2017, A&A, 601, A76
Kourniotis M., Kraus M., Arias M. L., Cidale L., Torres A. F., 2018, MNRAS, 480, 3706
Kourniotis M., Kraus M., Arias M. L., Cidale L. S., 2025, MNRAS, 540, L28
Kraus M., 2009, A&A, 494, 253
Kraus M., 2019, Galaxies, 7, 83
Kraus M., Krügel E., Thum C., Geballe T. R., 2000, A&A, 362, 158
Kraus M., Borges Fernandes M., de Araújo F. X., 2010, A&A, 517, A30
Kraus M., Oksala M. E., Nickeler D. H., Muratore M. F., Borges Fernandes M., Aret A., Cidale L. S., de Wit W. J., 2013, A&A, 549, A28
Kraus M., Cidale L. S., Arias M. L., Oksala M. E., Borges Fernandes M., 2014, ApJ, 780, L10
Kraus M. et al., 2016, A&A, 593, A112
Kraus M., Arias M. L., Cidale L. S., Torres A. F., 2020, MNRAS, 493, 4308
Kraus M., Kourniotis M., Arias M. L., Torres A. F., Nickeler D. H., 2023, Galaxies, 11, 76
Kurucz R. L., 1992, in Barbuy B., Renzini A., eds, IAU Symp. 149, The Stellar Populations of Galaxies. Kluwer Academic Publishers, Dordrecht, p. 225
Lambert D. L., Hinkle K. H., Hall D. N. B., 1981, ApJ, 248, 638
Lamers H. J. G. L. M., Zickgraf F.-J., de Winter D., Houziaux L., Zorec J., 1998, A&A, 340, 117
Li G., Gordon I. E., Rothman L. S., Tan Y., Hu S.-M., Kassi S., Campargue A., Medvedev E. S., 2015, ApJS, 216, 15

Liermann A., Kraus M., Schnurr O., Fernandes M. B., 2010, MNRAS, 408, L6
Luo A. L., Zhao Y. H., Zhao G. et al., 2022, VizieR Online Data Catalog: LAMOST DR7 catalogs. V/156
Mahy L. et al., 2022, A&A, 657, A4
Maravelias G., Kraus M., Cidale L. S., Borges Fernandes M., Arias M. L., Curé M., Vasilopoulos G., 2018, MNRAS, 480, 320
Maravelias G., Bonanos A. Z., Tramper F., de Wit S., Yang M., Bonfini P., 2022, A&A, 666, A122
Maravelias G., de Wit S., Bonanos A. Z., Tramper F., Munoz-Sanchez G., Christodoulou E., 2023, Galaxies, 11, 79
Marchant P., Bodensteiner J., 2024, ARA&A, 62, 21
Martin J. C., Humphreys R. M., 2017, AJ, 154, 81
Martins F., Palacios A., 2013, A&A, 560, A16
Masci F. J. et al., 2019, PASP, 131, 018003
Massey P., Bianchi L., Hutchings J. B., Stecher T. P., 1996, ApJ, 469, 629
Massey P., Olsen K. A. G., Hodge P. W., Strong S. B., Jacoby G. H., Schlingman W., Smith R. C., 2006, AJ, 131, 2478
Massey P., McNeill R. T., Olsen K. A. G., Hodge P. W., Blaha C., Jacoby G. H., Smith R. C., Strong S. B., 2007, AJ, 134, 2474
Massey P., Neugent K. F., Morrell N., Hillier D. J., 2014, ApJ, 788, 83
Massey P., Neugent K. F., Smart B. M., 2016, AJ, 152, 62
McGregor P. J., Hyland A. R., Hillier D. J., 1988a, ApJ, 324, 1071
McGregor P. J., Hillier D. J., Hyland A. R., 1988b, ApJ, 334, 639
McGregor P. J., Hyland A. R., McGinn M. T., 1989, A&A, 223, 237
Morris P. W., Eenens P. R. J., Hanson M. M., Conti P. S., Blum R. D., 1996, ApJ, 470, 597
Muratore M. F., de Wit W. J., Kraus M., Aret A., Cidale L. S., Borges Fernandes M., Oudmaijer R. D., Wheelwright H. E., 2012, in Carciofi A. C., Rivinius T., eds, ASP Conf. Ser. Vol. 464, Circumstellar Dynamics at High Resolution. Astron. Soc. Pac., San Francisco, p. 67
Muratore M. F., Kraus M., Oksala M. E., Arias M. L., Cidale L., Borges Fernandes M., Liermann A., 2015, AJ, 149, 13
Neugent K. F., 2021, ApJ, 908, 87
Neugent K. F., Levesque E. M., Massey P., 2018, AJ, 156, 225
Neugent K. F., Levesque E. M., Massey P., Morrell N. I., 2019, ApJ, 875, 124
Neugent K. F., Levesque E. M., Massey P., Morrell N. I., Drout M. R., 2020, ApJ, 900, 118
Oksala M. E., Kraus M., Arias M. L., Borges Fernandes M., Cidale L., Muratore M. F., Curé M., 2012, MNRAS, 426, L56
Oksala M. E., Kraus M., Cidale L. S., Muratore M. F., Borges Fernandes M., 2013, A&A, 558, A17
Oudmaijer R. D., de Wit W. J., 2013, A&A, 551, A69
Oudmaijer R. D., Davies B., de Wit W. J., Patel M., 2009, in Luttermoser D. G., Smith B. J., Stencel R. E., eds, ASP Conf. Ser. Vol. 412, The Biggest, Baddest, Coolest Stars. Astron. Soc. Pac., San Francisco, p. 17
Pantaleoni González M., Maíz Apellániz J., Barbá R. H., Negueruela I., 2020, RNAAS, 4, 12
Patrick L. R., Thilker D., Lennon D. J., Bianchi L., Schootemeijer A., Dorda R., Langer N., Negueruela I., 2022, MNRAS, 513, 5847
Patrick L. R., Lennon D. J., Schootemeijer A., Bianchi L., Negueruela I., Langer N., Thilker D., Dorda R., 2024, A&A 700 A36
Peacock M. B., Maccarone T. J., Knigge C., Kundu A., Waters C. Z., Zepf S. E., Zurek D. R., 2010, MNRAS, 402, 803
Plez B., 2012, Astrophysics Source Code Library, record ascl:1205.004
Sana H. et al., 2012, Science, 337, 444
Sarkisyan A. et al., 2020, MNRAS, 497, 687
Sholukhova O., Bizyaev D., Fabrika S., Sarkisyan A., Malanushenko V., Valeev A., 2015, MNRAS, 447, 2459
Sholukhova O. N. et al., 2024, Astrophys. Bull., 79, 373
Shporer A., Mazeh T., 2006, MNRAS, 370, 1429
Skrutskie M. F. et al., 2006, AJ, 131, 1163
Solovyeva Y. et al., 2019, MNRAS, 484, L24
Soraisam M. D. et al., 2018, ApJ, 859, 73
Szécsi D., Agrawal P., Wünsch R., Langer N., 2022, A&A, 658, A125
Szeifert T., Humphreys R. M., Davidson K., Jones T. J., Stahl O., Wolf B., Zickgraf F. J., 1996, A&A, 314, 131
Torres A. F., Cidale L. S., Kraus M., Arias M. L., Barbá R. H., Maravelias G., Borges Fernandes M., 2018, A&A, 612, A113
U. V., Urbaneja M. A., Kudritzki R.-P., Jacobs B. A., Bresolin F., Przybilla N., 2009, ApJ, 704, 1120
Valeev A. F., Sholukhova O., Fabrika S., 2009, MNRAS, 396, L21
van den Bergh S., Herbst E., Kowal C. T., 1975, ApJS, 29, 303
Walborn N. R., Fitzpatrick E. L., 2000, PASP, 112, 50
Weis K., Bomans D. J., 2020, Galaxies, 8, 20
Wittkowski M. et al., 2017, A&A, 606, L1
Yershov V. N., 2014, Ap&SS, 354, 97
Yusof N. et al., 2022, MNRAS, 511, 2814

This paper has been typeset from a TEX/LATEX file prepared by the author.